

Properties of doubly-excited states of Li^- and Be : The study of electron correlations in hyperspherical coordinates

C D Lin

Department of Physics, Kansas State University, Manhattan, Kansas 66506, USA

Received 14 September 1982

Abstract. By adopting a frozen-core approximation with the two valence electrons treated in suitably chosen model potentials, the correlations of doubly-excited states of Li^- and Be are studied in hyperspherical coordinates in the adiabatic approximation. The characteristics of correlation patterns for these states are found to be similar to those for the corresponding states of H^- and He except for the gradual loss of the strong angular correlation for Li^- and Be at large hyper-radius. Adiabatic potential curves and eigen-energies for the doubly-excited states lying below the $n=2$ and $n=3$ limits of the one-electron ions are calculated and compared with results from the configuration interaction method using the same model potential to assess the validity of the adiabatic approximation. It is concluded that for certain $\{L, S, \pi\}$ states the adiabatic approximation is quite adequate but for others, e.g., $^1\text{P}^\circ$, couplings between neighbouring channels are important.

1. Introduction

Hyperspherical coordinates have been used in recent years to study correlations between two excited electrons in H^- and He (Lin 1982a, b, and references therein; Fano 1983). Many interesting properties of doubly-excited states have been revealed in these studies. While these prototype systems provide characteristics of doubly-excited states in two-electron systems, it is important to examine whether these characteristics also exist in doubly-excited states of many-electron systems.

The simplest many-electron systems of this type are alkali negative ions and alkaline-earth atoms. In these systems, the electron pair of interest are attracted to a spherically symmetric ionic core, when both electrons of the pair remain outside the core radius. Under this restriction, the electron pair experiences primarily an attractive Coulomb potential plus a weaker polarisation potential. On the other hand, penetration of either electron within the core exposes the electron to a stronger field and to substantial exchange of energy and angular momentum with the core electrons. These effects are minimal for two-valence-electron systems where the core can be regarded as 'frozen'. Therefore, these systems can be treated in hyperspherical coordinates similar to H^- and He except that the electron–nucleus interaction is replaced by a non-Coulombic local potential $V(r)$.

A previous investigation by Greene (1981) along these lines chose $V(r)$ to be the Herman–Skillman (1963) potential. It is known that this potential does not represent the valence-electron–core interaction accurately. Thus some of his quantitative results are inferior to the conventional state-of-the-art calculations and the results could be

easily misinterpreted as the failure of the approach based upon hyperspherical coordinates. In this paper we adopt a more accurate model potential to represent the two-valence-electron systems, Li^- and Be . We will show that the qualitative conclusions of Greene (1981) are still valid while the quantitative results are significantly improved. We also propose a more effective method of calculating adiabatic potential curves by generalising the analytical channel functions developed for H^- and He (Lin 1981) to these model two-electron systems.

With this modification our object here is to solve the model two-electron systems in hyperspherical coordinates in the adiabatic approximation similar to the earlier treatments for H^- and He . The non-Coulomb character of the model potential $V(r)$ breaks the degeneracy of the limiting values of the potential curves, $U_\mu(R \rightarrow \infty)$. Lack of this degeneracy constricts the development of strong angular correlation at large hyper-radius R because the exchange of angular momentum between the two electrons requires energy transfer—in contrast to H^- and He where the exchange requires no energy transfer owing to the degeneracy of $\text{H}(nl)$ and $\text{He}^+(nl)$ ($n \geq 2$) spectra (Lin 1982b). In the region of intermediate hyperspherical radius R , energy exchange between the electron pair is large and a strong angular correlation can be easily developed. In this region, the correlation patterns for the pair of valence electrons in Li^- and Be are expected to behave like the pair of electrons in H^- and He . Our goal here is to elucidate the evolution of the two electrons from the correlated regime at small R to the uncorrelated regime at large R .

In § 2, we summarise the model potential approach of Dalgarno, Laughlin, Victor and co-workers. Calculations of adiabatic potential curves in hyperspherical coordinates are described in § 3 and the results of applications to Li^- and Be are presented in § 4. We use atomic units unless otherwise noted.

2. Model potentials for two-valence-electron systems

The model potentials used here follow the work of Laughlin and Victor (1972). Consider an $(N+2)$ -electron system having two valence electrons outside a closed-shell polarisable core. Assuming that the core electrons follow the motion of the valence electrons instantaneously and neglect the exchange between valence and core electrons, the total wavefunction for the system may be written in the adiabatic approximation

$$\psi = \psi_c(\mathbf{r}; \mathbf{r}_1, \mathbf{r}_2) \psi_v(\mathbf{r}_1, \mathbf{r}_2) \quad (1)$$

where the core wavefunction ψ_c depends parametrically on the coordinates of the two valence electrons \mathbf{r}_1 and \mathbf{r}_2 , and \mathbf{r} labels, collectively, the position vectors of the N core electrons. Allowing \mathbf{r}_1 and \mathbf{r}_2 to vary and assuming that both r_1 and r_2 are larger than the radius of each core electron, one obtains the equation for the two valence electrons,

$$\left(-\frac{1}{2}\nabla_1^2 - \frac{1}{2}\nabla_2^2 + V(r_1) + V(r_2) + V_{12}\right) \phi_v(\mathbf{r}_1, \mathbf{r}_2) = E_v \phi_v(\mathbf{r}_1, \mathbf{r}_2). \quad (2)$$

The valence-electron-core interaction takes the form

$$V(r) = -\frac{Z}{r} + V_c^{\text{HF}}(r) - \frac{\alpha_d}{2r^4} W_4\left(\frac{r}{r_0}\right) - \frac{\alpha_q}{2r^6} W_8\left(\frac{r}{r_0}\right) + U(r; a) \quad (3)$$

where V_c^{HF} is the core potential computed from the Hartree-Fock ground-state

orbitals, α_d (α_q) is the dipole (quadrupole) polarisability and

$$W_n = 1 - \exp(-x^n)$$

is the cut-off function, with cut-off radius r_0 . The last term $U(r; a)$ is predominantly a short-range correction term which depends on a set of parameters. Following Laughlin and Victor (1972),

$$U(r; a) = (a_0 + a_1 r + a_2 r^2) \exp(-kr) + (a'_0 + a'_1 r) \exp(-k'r). \quad (4)$$

These short-range parameters as well as the cut-off radius r_0 are determined so that the spectrum of the one-electron equation

$$\left(-\frac{1}{2}\nabla^2 + V(r)\right)\phi_j(\mathbf{r}) = \varepsilon_j \phi_j(\mathbf{r}) \quad (5)$$

reproduces the experimental singly-excited states for the one-valence-electron system.

The electron-electron interactions, V_{12} are taken to be

$$V_{12} = \frac{1}{r_{12}} - \frac{\alpha_d}{r_1^2 r_2^2} P_1(\cos \theta_{12}) W_3\left(\frac{r_1}{r_0}\right) W_3\left(\frac{r_2}{r_0}\right) - \frac{\alpha'_q}{r_1^3 r_2^3} P_2(\cos \theta_{12}) W_4\left(\frac{r_1}{r_0}\right) W_4\left(\frac{r_2}{r_0}\right). \quad (6)$$

In this work the model potential parameters for Li are taken from Victor and Laughlin (1972), and for Be^+ from Laughlin and Victor (1972).

3. Hyperspherical coordinates approach

Equation (2) has been solved for many two-valence electron systems by the conventional configuration interaction method (CI). A similar model potential approach (but with a different parametrisation) has also been used by Moore and Norcross (1974) where equation (2) is solved by the close-coupling expansion. In this article we solve equation (2) in hyperspherical coordinates in the adiabatic approximation.

The two-valence-electron wavefunctions $\Psi_v(\mathbf{r}_1, \mathbf{r}_2)$ are expressed in hyperspherical coordinates in the adiabatic approximation as

$$\Psi_v(\mathbf{r}_1, \mathbf{r}_2) = (R^{5/2} \sin \alpha \cos \alpha)^{-1} F_\mu^n(R) \Phi_\mu(R; \Omega) \quad (7)$$

for the n th state in channel μ . The channel function Φ_μ satisfies

$$\left(-\frac{1}{R^2} \frac{d^2}{d\alpha^2} + (V_1 + V_2 + V_{12})\right) \Phi_\mu(R; \Omega) = \bar{U}_\mu(R) \Phi_\mu(R; \Omega) \quad (8)$$

and the eigen-energies E_μ^n for the n th state of channel μ are obtained in the adiabatic approximation from the radial equation

$$\left(\frac{d^2}{dR^2} + (2E_\mu^n - U_\mu(R))\right) F_\mu^n(R) = 0 \quad (9)$$

where

$$U_\mu(R) = \bar{U}_\mu(R) - W_{\mu\mu}(R) \quad (10)$$

and

$$W_{\mu\mu}(R) = \left\langle \Phi_\mu(R; \Omega), \frac{d^2}{dR^2} \Phi_\mu(R; \Omega) \right\rangle \quad (11)$$

is the diagonal non-adiabatic term.

For real two-electron problems, equation (8) has been solved using various methods: (i) by direct numerical integration (Macek 1968, Greene 1981); (ii) by diagonalisation using hyperspherical harmonics as basis functions (Lin 1974, Klar and Klar 1978); (iii) by finite-difference method (Lin 1975) and (iv) most efficiently, in terms of linear combinations of hyperspherical harmonics and analytical channel functions (Lin 1981). The last method has the advantage of numerical stability and convergence since basis functions suitable for small R and for large R are both included. Recent works on H^- and He in hyperspherical coordinates have shown the usefulness of this approach.

To generalise the method of analytical channel functions developed earlier for H^- and He (Lin 1981) to the present situation, we solve the one-electron orbital $\phi_q(\mathbf{r})$ from (5) in terms of linear combinations of Slater-type orbitals

$$\phi_q(\mathbf{r}) = \sum_i \alpha_i^q r^{n_i-1} \exp(-\beta_i r) Y_{l_i m_i}(\hat{\mathbf{r}}). \quad (12)$$

The one-electron binding energies obtained from the model potentials of Victor and Laughlin (1972) for Li and of Laughlin and Victor (1972) for Be^+ , as shown in table 1, are in good agreement with the experimental energies.

Table 1. Comparison of the eigenvalues of the model potentials with experimental binding energies of Li and Be^+ (given in rydbergs).

	Li		Be^+	
	Theory	Experimental ^a	Theory	Experimental ^a
2s	-0.398 75	-0.396 32	-1.3394	-1.3382
3s	-0.148 90	-0.148 38	-0.5347	-0.5342
4s	-0.077 19	-0.077 24	-0.2855	-0.2860
2p	-0.260 65	-0.260 50	-1.0494	-1.0472
3p	-0.114 55	-0.114 48	-0.4589	-0.4588
4p	-0.063 93	-0.063 95	-0.2549	-0.2560
3d	-0.111 24	-0.111 22	-0.4447	-0.4446
4d	-0.062 54	-0.062 55	-0.2497	-0.2500
4f	-0.062 50	-0.062 51	-0.2498	-0.2498

^aFrom Moore (1949).

Following Lin (1981), the analytical channel functions within each $[l_1 l_2]$ pair are generalised as follows.

(a) For $l_1 = l_2 = l$, assuming that the r -weighted radial wavefunction of (5) is

$$F_q(r) = \sum_i a_i^q r^{n_i} \exp(-\beta_i r)$$

the α -dependent part of the analytical channel function at each R is obtained by replacing r by $R \sin \alpha \cos \alpha$ to give

$$\phi_{llq}(R \sin \alpha \cos \alpha) = N(R) \sum_i a_i^q (R \sin \alpha \cos \alpha)^{n_i} \exp(-\beta_i R \sin \alpha \cos \alpha) \quad (13)$$

and the analytical channel function is $\phi_{llq}(R \sin \alpha \cos \alpha) Y_{llM}(\mathbf{r}_1, \mathbf{r}_2)$ where $Y_{l_1 l_2 LM}(\hat{\mathbf{r}}_1, \hat{\mathbf{r}}_2)$ is the coupled angular momentum wavefunction of the two electrons.

The normalisation in (13) is chosen such that

$$\int_0^{\pi/2} |\phi_{llq}(R \sin \alpha \cos \alpha)|^2 d\alpha = 1. \quad (14)$$

(b) For $l_1 \neq l_2$ where l_1 is the angular momentum quantum number of the inner electron, the analytical channel function is

$$\phi_{l_1 l_2 q} = N(R) A \left(\sum_i a_i^q (R \sin \alpha)^{n_i} \exp(-\beta_i R \sin \alpha) Y_{l_1 l_2 LM}(\hat{r}_1, \hat{r}_2) \right) \quad (15)$$

where A is the proper (anti-) symmetrisation operator.

In terms of these analytical channel functions and hyperspherical harmonics, equation (8) can be easily solved accurately using a small basis set (< 15). The resulting potential curves $U_\mu(R)$ are used to calculate the binding energies (see equation (9)) as well as for the classification of doubly-excited states in Li^- and Be . The behaviour of $\Phi_\mu(R; \Omega)$ over Ω at each R serves to illustrate the evolution of correlation patterns of two excited electrons in Li^+ or Be^{2+} core.

4. Results and discussion

4.1. Correlations of doubly-excited states of Be

4.1.1. *Correlation patterns for $1,3S^e$ states.* The two adiabatic potential curves for $1,3S^e$ states of Be converging to the $2s$ and $2p$ states of Be^+ are shown in figure 1. They are labelled in terms of quantum numbers of the inner electron and the orbital angular momentum quantum number of the outer electron in the asymptotic limit ($R \rightarrow \infty$). These conventional designations do not reflect the strong radial and angular correlations of the two electrons in the small- R region.

The shape of the potential curves shown in figure 1 are very similar to the corresponding ones in the doubly-excited states of He (Macek 1968, Lin 1974).

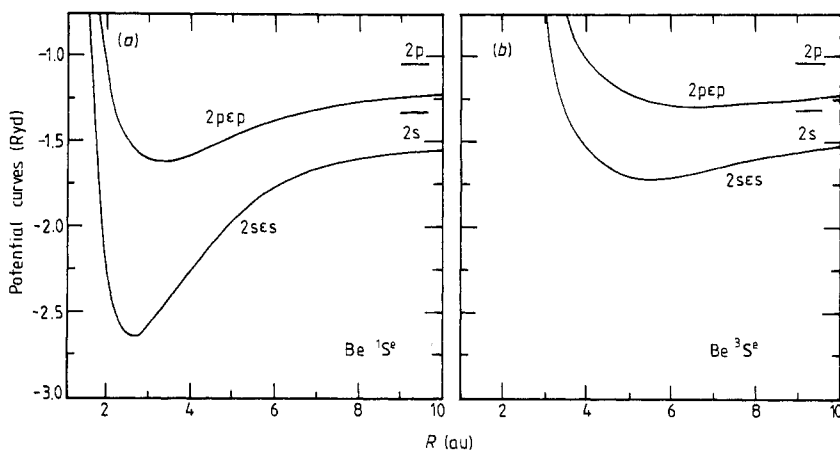


Figure 1. Adiabatic potential curves of (a) $\text{Be } 1S^e$ and (b) $\text{Be } 2S^e$ channels converging to $\text{Be}^+(2s)$ and $\text{Be}^+(2p)$ limits. The channels are labelled using the quantum numbers according to the independent-electron approximation.

However, there is one major difference: because of the degeneracy of 2s and 2p states in He^+ , there is strong angular coupling between $2s\epsilon s^1S$ and $2p\epsilon p^1S$ in He even at large hyper-radius R , while the lack of degeneracy between the 2s and 2p states of Be^+ results in the absence of such angular mixing at large R . This difference also results in some variation in the correlation patterns of doubly-excited states in Be as compared with those in He.

To illustrate the correlation patterns, we show in figure 2 the surface charge density plots $|\Phi_\mu(R; \alpha, \theta_{12})|^2$ on the (α, θ_{12}) plane for the $2s\epsilon s^1S^e$ and $2p\epsilon p^1S^e$ channels of Be at four different values of R . These plots are to be compared with the corresponding ones in H^- , as shown in figure 6 of Lin (1982a). These graphs are shown at different orientations for the two channels to exhibit greater detail. We notice that the graphs at $R = 2$ and $R = 6$ show the characteristics of doubly-excited states belonging to these two channels, namely, that the correlation pattern for the lower channel exhibits a strong peak near $\alpha = 45^\circ$ and $\theta_{12} = 180^\circ$, and with a large charge concentration in the $\theta_{12} > 90^\circ$ region while the correlation pattern for the upper channel exhibits a pronounced nodal line near $\theta_{12} \sim 90^\circ$ and with a relatively large charge concentration in the region of $\theta_{12} < 90^\circ$. In this respect, doubly-excited states in Be have similar correlation patterns as in the corresponding states in He and H^- . Within a given channel, the charge density near $\alpha = 45^\circ$ drops as R increases with the inner electron remaining

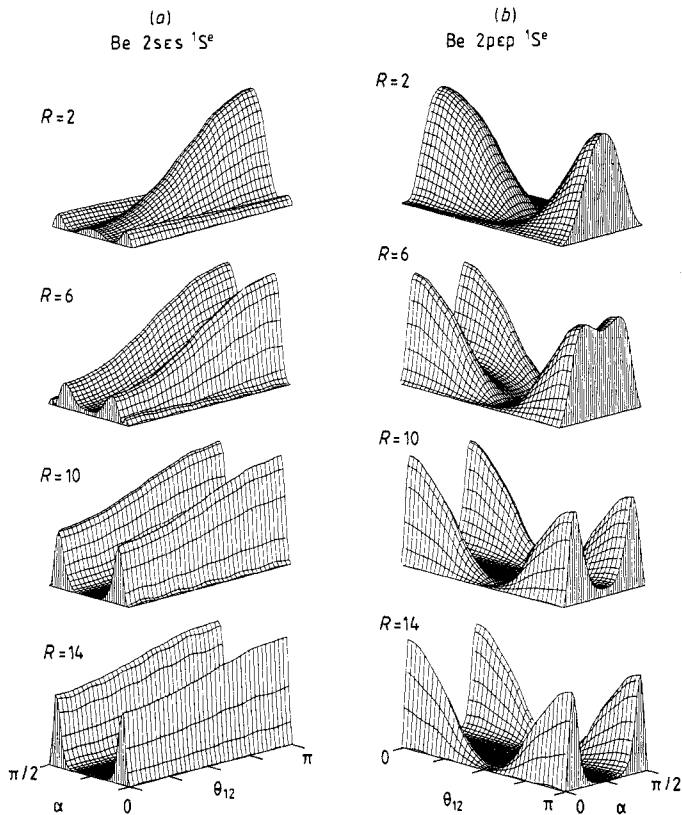


Figure 2. Plots of surface charge densities of (a) $\text{Be } 2s\epsilon s^1S^e$ and (b) $2p\epsilon p^1S^e$ channels on the θ_{12} plane at four different values of R . Notice that the orientations are different for the two channels.

near the core and the outer one moving out. This is reflected by the depression in the surface charge density plots around the $\alpha = 45^\circ$ line (see figure 2 and also figure 6 of Lin (1982a)) at large R . However, there is an important difference occurring at large R . In H^- , as well as in He , the depression near $\alpha = 45^\circ$ at increasing values of R is *not* accompanied by any significant change in the angular correlation pattern. This was clearly illustrated in figures 6 of Lin (1982a) as well as in figure 5 of Lin (1982b) where the 'average' $\langle \theta_{12} \rangle$ was found to be essentially constant for each channel. We notice that the angular correlation pattern for the $2s\epsilon s \ ^1S^e$ channel changes gradually as R increases. Instead of concentrating only in the $\theta_{12} > 90^\circ$ region, the charge distribution spreads out to the whole θ_{12} region at large R . At $R = 14$, we notice that there is no pronounced angular correlation between the two electrons—as characterised by the $2s\epsilon s \ ^1S^e$ designation. On the other hand, by referring to figure 1(a), we found that such a lack of angular correlations occurs only at R values far away from where the potential well lies. Therefore, we can expect states localised near the potential well to show strong angular correlations, while higher Rydberg states, which are localised far away from the potential well, show less overall angular correlation. This behaviour is well known from the conventional configuration interaction (CI) studies where the ground state of Be was shown to have large CI coefficients involving configurations like $2p^2 \ ^1S^e$ and $3d^2 \ ^1S^e$, but such mixing is very small for the states $2sn s \ ^1S$ ($n \geq 3$). The variation of angular correlation is less conspicuous for the $2p\epsilon p \ ^1S^e$ channel because there is already some angular correlation implied by the $2p\epsilon p \ ^1S^e$ designation (where the charge density varies as $\cos^2 \theta_{12}$).

The angular correlation patterns do not depend significantly on the spin quantum numbers. In figure 3 we show the surface charge density plots for the $2s\epsilon s \ ^3S^e$ and $2p\epsilon p \ ^3S^e$ channels of Be . Except for the fixed nodal line along $\alpha = 45^\circ$, there is little difference between the corresponding plots. A similar behaviour in H^- has been illustrated earlier (Lin 1982a).

We summarise this subsection by stating that the correlation patterns of $2s\epsilon s \ ^1S^e$ and $2p\epsilon p \ ^1S^e$ states are similar to those in the corresponding channels in He and H^- at small hyper-radius, but are similar to those predicted by the independent-electron approximation at large hyper-radius. These states thus exhibit properties characteristic of doubly-excited states at small hyper-radius and of independent electrons at large hyper-radius.

4.1.2. Eigen-energies for $^{1,3}S^e$ states. The energies of the few lowest states for $2s\epsilon s \ ^{1,3}S^e$ and $2p\epsilon p \ ^{1,3}S^e$ channels of Be calculated in the adiabatic approximation using the potential curves shown in figure 1 are tabulated in table 2, together with the results from the configuration-mixing calculations and with experimental results. The energies are given in rydbergs with respect to the Be^{2+} threshold. Also in the table are the quantum defects for the states indicated with respect to their respective thresholds. In general, we notice that the binding energies for $2sn s \ ^{1,3}S^e$ states predicted using the present adiabatic approximation are slightly above those calculated using the configuration interaction (CI) method, whereas the reverse is true for $2pn p \ ^{1,3}S^e$ series. The experimental binding energies for $2sn s \ ^{1,3}S^e$ states are lower than both predictions. We also notice that the quantum defects computed from the present adiabatic approximation deteriorate along the $2sn s \ ^1S^e$ series.

The above results are consistent with the earlier conclusions for H^- and He , that the adiabatic approximation becomes less valid with an increasing degree of excitation. The inclusion of non-adiabatic couplings between $2sn s \ ^1S^e$ and $2pn p \ ^1S^e$ channels is

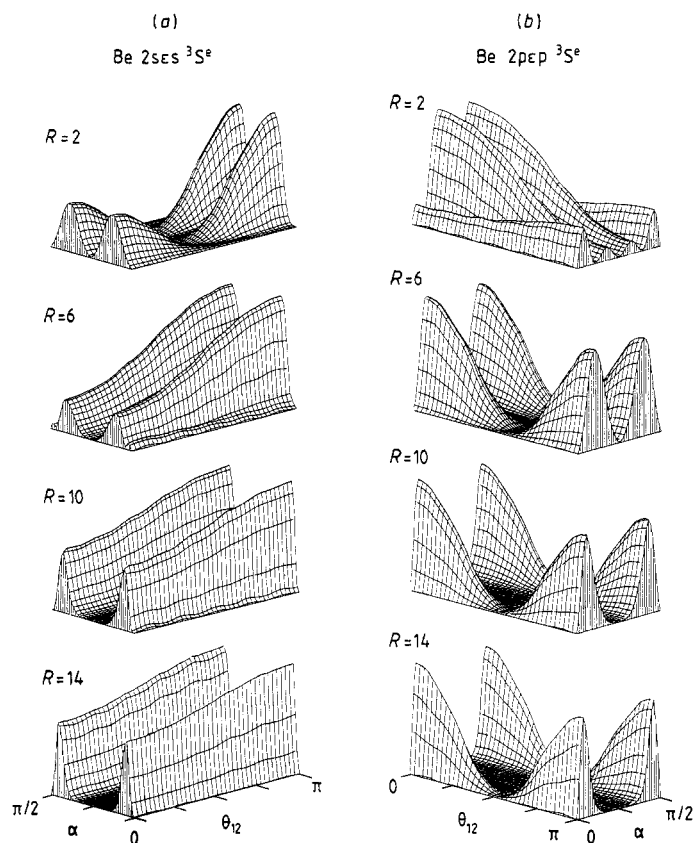


Figure 3. Plots of surface charge densities of (a) Be $2s\epsilon s\ ^3S^e$ and (b) $2p\epsilon p\ ^3S^e$ channels on the θ_{12} plane at four different values of R .

Table 2. Eigen-energies and quantum defects of $1,3S^e$ doubly-excited states of Be.

State	Eigen-energies			Quantum defects		
	Hyper-spherical	Model potential ^a	Experimental ^b	Hyper-spherical	Model potential ^a	Experimental ^b
$2s^2\ ^1S^e$	-2.0171	-2.0185	-2.0238	0.785	0.786	0.792
$2s3s\ ^1S^e$	-1.5149	-1.5236	-1.5255	0.613	0.670	0.684
$2s4s\ ^1S^e$	-1.4239	-1.4284	-1.4292	0.560	0.648	0.685
$2p^2\ ^1S^e$	-1.3196	-1.3102		0.076	0.041	
$2p3p\ ^1S^e$	-1.1557			0.067		
$2s3s\ ^3S^e$	-1.5447	-1.5478	-1.5492	0.793	0.809	0.823
$2s4s\ ^3S^e$	-1.4327	-1.4352	-1.4360	0.726	0.769	0.802
$2p3p\ ^3S^e$	-1.1932			0.363		

^a Laughlin and Victor (1972).

^b Moore (1949).

expected to improve the numerical results significantly. Notice that the energies are too high for $2sns\ ^1S^e$ series but too low for $2pn p\ ^1S^e$ series (as compared with the CI results). The introduction of coupling, according to the general behaviour of 'spectral

repulsion', will bring both series in better agreement with other more accurate calculations and with experiments. Notice that the non-adiabatic effects for the $2sn\text{s } ^1,^3\text{S}^e$ series are expected to increase with higher values of n .

The $2\text{s}^2\ ^1\text{S}^e$ binding energy predicted within the present adiabatic approximation is 0.677 Ryd, as compared with the value of 0.679 Ryd computed by the CI method using the same model potential. Both are in reasonably good agreement with the experimental value, 0.685 Ryd. The present result is a significant improvement over the earlier value 0.740 Ryd given by Greene. In this work, Greene used a less accurate potential for the model two-electron system and the diagonal non-adiabatic coupling term $W_{\mu\mu}$ (see equation (11)) was not included in his adiabatic potential. We thus point out that an adequate binding energy for $\text{Be } 2\text{s}^2\ ^1\text{S}^e$ can still be obtained within the adiabatic approximation if a realistic model potential is used.

4.1.3. $^1,^3\text{P}^o$ States. The potential curves for the $^1,^3\text{P}^o$ states of Be converging to the 2s and 2p limits of Be^+ are shown in figure 4. There is a strong avoided crossing between the $2\text{s}\epsilon\text{p}$ and $2\text{p}\epsilon\text{s}$ curves for $^1\text{P}^o$ at $R \sim 5.0$. This behaviour is different from the corresponding + and - curves in He where a diabatic crossing occurs at $R \sim 7.5$. This difference originates from the lack of strong angular coupling between the $2\text{s}\epsilon\text{p}$ and $2\text{p}\epsilon\text{s}$ channels in the large- R region owing to the non-degeneracy of the $\text{Be}^+(2\text{s})$ and $\text{Be}^+(2\text{p})$ states. The strong non-adiabatic coupling suggests that the breakdown of the adiabatic approximation will be quite severe for $^1\text{P}^o$ states. Such non-adiabatic coupling has been considered by Greene (1981) recently.

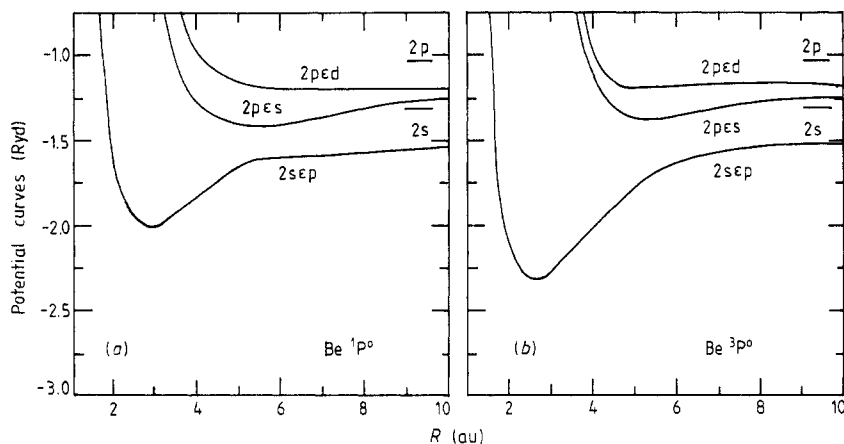


Figure 4. Adiabatic potential curves of (a) $\text{Be } ^1\text{P}^o$ and (b) $\text{Be } ^3\text{P}^o$ channels converging to the $\text{Be}^+(2\text{s})$ and $\text{Be}^+(2\text{p})$ limits. Notice the strong avoided crossing between the $2\text{s}\epsilon\text{p}$ $^1\text{P}^o$ and $2\text{p}\epsilon\text{s}$ $^1\text{P}^o$ channels at $R \sim 5$ au.

In table 3 we present the eigen-energies and quantum defects of the low-lying states of each $^1,^3\text{P}^o$ channel using the potential curves shown in figure 4. For $^1\text{P}^o$, we notice that the quantum defects for $2sn\text{p } ^1\text{P}^o$ states differ from the corresponding ones calculated in the CI method using the same model potential by as much as 0.2. Although these adiabatic values are slightly better than those obtained by Greene,

Table 3. Eigen-energies and quantum defects of $^{1,3}P^{\circ}$ excited states of Be.

State	Eigen-energies			Quantum defects			
	Hyper-spherical	Model potential ^a	Experimental ^b	Hyper-spherical	Model potential ^a	Experimental ^b	Greene ^c
2s2p $^1P^{\circ}$	-1.6122	-1.6210	-1.6359	0.085	0.115	0.167	-0.021
2s3p $^1P^{\circ}$	-1.4531	-1.4670	-1.4753	0.034	0.201	0.299	0.007
2s4p $^1P^{\circ}$	-1.4024	-1.4108	-1.4120	0.016	0.257	0.318	0.005
2p3s $^1P^{\circ}$	-1.2528	-1.2321	-1.2314	0.783	0.661	0.669	
2p4s $^1P^{\circ}$	-1.1423	-1.1325	-1.1384	0.719	0.531	0.688	
2p3d $^1P^{\circ}$	-1.1522	-1.1490	-1.1468	0.881	0.831	0.799	
2p4d $^1P^{\circ}$	-1.1076	-1.1027	-1.1019	0.855	0.668	0.638	
2s2p $^3P^{\circ}$	-1.8143	-1.8143	-1.8235	0.549	0.549	0.564	
2s3p $^3P^{\circ}$	-1.4724	-1.4840	-1.4869	0.258	0.370	0.407	
2s4p $^3P^{\circ}$	-1.4090	-1.4135	-1.4149	0.210	0.326	0.390	
2p3s $^3P^{\circ}$	-1.2371			0.692			
2p4s $^3P^{\circ}$	-1.1522			0.635			
2p3d $^3P^{\circ}$	-1.1532			-0.104			
2p4d $^3P^{\circ}$	-1.1080			-0.131			

^a Laughlin and Victor (1972).^b Moore (1949).^c Greene (1981).

this large discrepancy indicates the importance of incorporating non-adiabatic couplings in this case. Notice that the energies for $2pns\ ^1P^{\circ}$ states are lower than those calculated in the CI method. The introduction of non-adiabatic couplings with the $2snp\ ^1P$ channel is expected to push the $2pns\ ^1P^{\circ}$ energies up in accordance with the principle of spectral repulsion, thus resulting in a better agreement with the CI results.

Table 3 also gives the eigen-energies and quantum defects for the $^3P^{\circ}$ states. Although there is no discernable avoided crossing between $2sep$ and $2pes$ curves in figure 4(b), the non-adiabatic effect is not very small for the higher states. While the $2s2p\ ^3P^{\circ}$ energy calculated in the adiabatic approximation is in agreement with the CI result, the quantum defects for $2s3p$ and $2s4p$ are less accurate.

4.2. Doubly-excited states of Li^{-}

4.2.1. Potential curves converging to 2s and 2p limits of Li^{-} . The potential curves for $^{1,3}S^e$ and $^{1,3}P^{\circ}$ states of Li^{-} converging to the 2s and 2p limits of Li are shown in figure 5. Except for the $2s\epsilon s\ ^1S^e$ and $2sep\ ^3P^{\circ}$ curves, all the other curves are mostly repulsive. It turns out that the attractive $2sep\ ^3P^{\circ}$ curve is not strong enough to support any bound state. The $2s\epsilon s\ ^1S^e$ curve does support one bound state, corresponding to the $2s^2\ ^1S^e$ ground state of Li^{-} . The binding energy calculated under the adiabatic approximation is $-0.585\ eV$, as compared with $-0.594\ eV$ from the CI method and with the experimental value of $-0.596\ eV$. We also notice that the strong avoided crossing for $^1P^{\circ}$ curves in Be in figure 4 is also evident in the $^1P^{\circ}$ curves for Li^{-} .

The potential curves shown in figure 5 are to be compared with the corresponding ones in H^{-} (Lin 1976). Because of the non-degeneracy in the $Li(2s)$ and $Li(2p)$ limits, there is a lack of strong angular correlation at large R . The lack of such an angular correlation at large R results in the absence of additional diffuse bound states in Li.

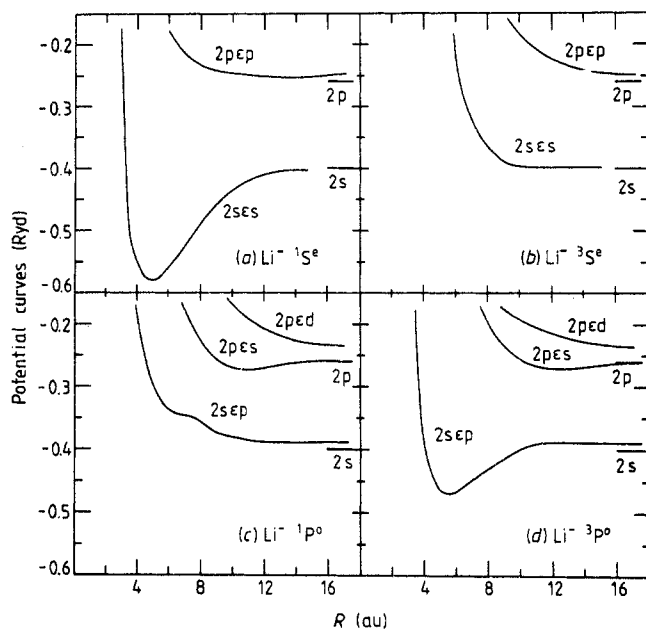


Figure 5. Adiabatic potential curves of (a) $\text{Li}^- 1S^e$, (b) $\text{Li}^- 3S^e$, (c) $\text{Li}^- 1P^o$ and (d) $\text{Li}^- 3P^o$ channels converging to the $\text{Li}(2s)$ and $\text{Li}(2p)$ limits respectively. Only $2s\epsilon s 1S^e$ curve is attractive enough to support a bound state.

4.2.2. Doubly-excited states of Li^- below the $\text{Li}(n=3)$ limits. To examine the qualitative behaviour of higher doubly-excited states in Li^- and to compare with the corresponding states in H^- studied earlier (Lin 1982b), we show in figure 6 the higher $1,3S^e$ potential curves of Li^- . These curves are to be compared with figure 1 of Lin (1982b). Except for the detailed behaviour in the asymptotic region, the shape of each curve and the diabatic crossings (between $3d\epsilon d 1S^e$ and $4s\epsilon s 1S^e$ in Li^- and between 3c and 4a in H^-) are also very similar. This implies that the properties of doubly-excited states of H^- studied earlier are expected to be true for the doubly-excited states of Li^- except for the gradual loss of angular correlations at large R . The lowest three $1,3P^o$ curves converging to the $\text{Li}(n=3)$ thresholds are shown in figure 7. These curves are similar to the corresponding curves for H^- shown in figures 2(a), 2(b) of Lin (1982b).

Within the adiabatic approximation, the eigen-energies calculated from the attractive potential curves in figures 6 and 7 are given in table 4. They are compared with the CI calculations of Stewart *et al* (1974) using the same model potential. Except for $3s3p 1P^o$, the calculated energies are in reasonable harmony. The large discrepancy for $3s3p 1P^o$ is an indication that the diabatic crossing assumed in figure 7(a) is not entirely satisfactory. To improve the accuracy, it is desirable to take into account the coupling between the $3s\epsilon p$ and $3p\epsilon s$ channels.

5. Conclusions

In this paper we have illustrated the study of doubly-excited states of two-valence-electron systems in hyperspherical coordinates. It is shown that accurate results

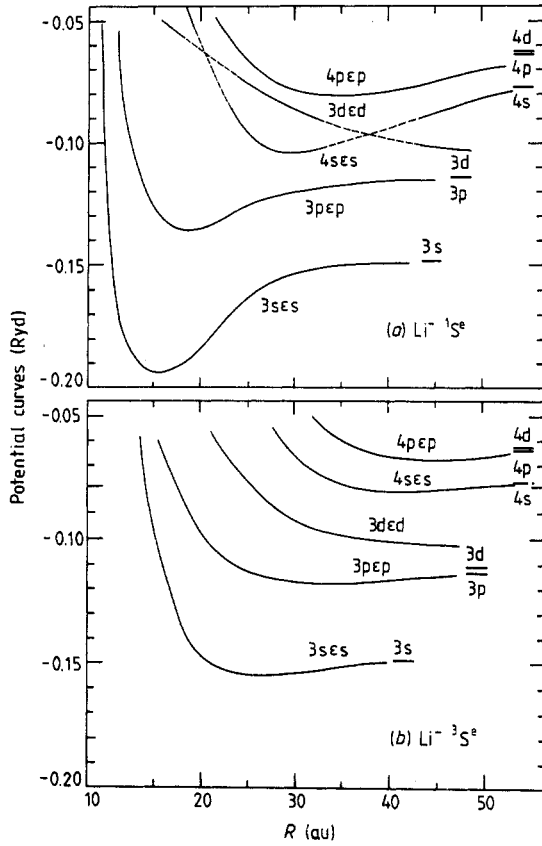


Figure 6. Potential curves for (a) the $\text{Li}^{-1}\text{S}^{\circ}$ and (b) the $\text{Li}^{-3}\text{S}^{\circ}$ channels converging to the $\text{Li}(n=3)$ and $\text{Li}(n=4)$ limits.

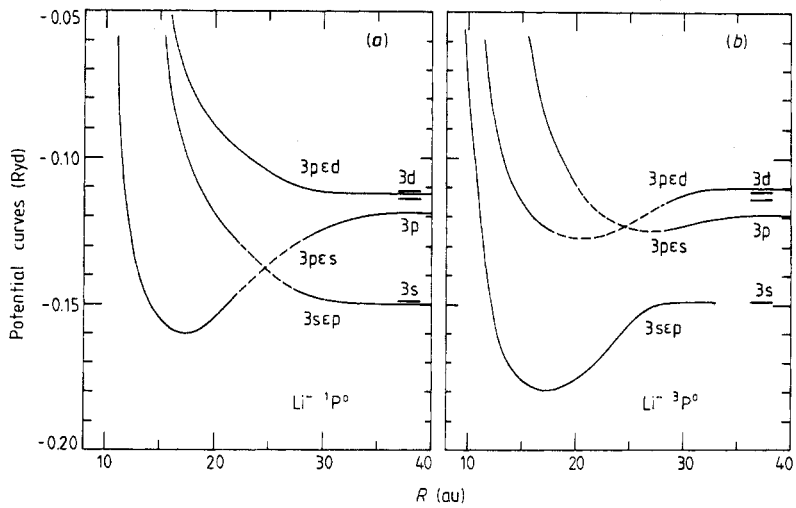


Figure 7. Potential curves for (a) $\text{Li}^{-1}\text{P}^{\circ}$ and (b) $\text{Li}^{-3}\text{P}^{\circ}$ channels converging to $\text{Li}(n=3)$ limits.

Table 4. Eigen-energies (in rydbergs) of autoionising states in Li^- .

State	Hyperspherical	Model potential ^a
$3s^2\ ^1S^e$	-0.1667	-0.1688
$3p^2\ ^1S^e$	-0.1194	-0.1244
$3s4s\ ^1S^e$	-0.1484	-0.1486
$3p4p\ ^1S^e$	-0.1184	-0.1148
$3s3p\ ^1P^o$	-0.1342	-0.1188
$3s3p\ ^3P^o$	-0.1557	-0.1574
$4s^2\ ^1S^e$	-0.0913	—
$4p^2\ ^1S^e$	-0.0719	—

^a Stewart *et al* (1974).

comparable with those obtained in H^- and He can be obtained for these systems, with a few exceptions, within the adiabatic approximation if the model two-electron Hamiltonian is chosen accurately. The adoption of hyperspherical coordinates allows us to study the correlation patterns of doubly-excited states in many-electron systems. We have shown that the basic correlation patterns in these systems are similar to the corresponding states in H^- and He except for the loss of strong angular correlations at large hyperspherical radius. (The large angular correlation for doubly-excited states in H^- and He at large R is due to the degeneracy of the $\text{H}(n)$ and $\text{He}^+(n)$ cores when $n \geq 2$.)

We have also illustrated the situations where the adiabatic approximation fails. Our conclusions here are identical to those of the early work of Greene (1981). To obtain reasonable 'first-order' results for $^1P^o$ states, for example, it is necessary to couple at least the $2s\epsilon p$ and $2p\epsilon s$ channels. The strong coupling between these two channels explains the large autoionisation rates for the $2pn s\ ^1P^o$ states (Greene 1981, Fano 1983).

The implementation of analytical channel functions for calculations in hyperspherical coordinates simplifies the numerical work significantly. It is expected that these types of approaches can be further explored to study not only the qualitative aspects of spectroscopy, but also provide more accurate quantitative results.

Acknowledgment

This work is supported in part by the US Department of Energy, Division of Chemical Sciences and in part by the Alfred P Sloan Foundation.

References

- Fano U 1983 *Rep. Prog. Phys.* submitted
 Greene C H 1981 *Phys. Rev. A* **23** 661-78
 Herman F and Skillman S 1963 *Atomic Structure Calculations* (Englewood Cliffs, NJ: Prentice-Hall).
 Klar H and Klar M 1978 *Phys. Rev. A* **17** 1007-10
 Laughlin C and Victor G A 1972 *Atomic Physics* vol 3, ed S J Smith and G K Waters (New York: Plenum)
 Lin C D 1974 *Phys. Rev. A* **10** 1986-2001
 — 1976 *Phys. Rev. A* **14** 30-5

— 1981 *Phys. Rev. A* **23** 1585-90

— 1982a *Phys. Rev. A* **25** 76-87

— 1982b *Phys. Rev. A* **25** 1535-45

Macek J H 1968 *J. Phys. B: At. Mol. Phys.* **1** 831-43

Moore C E 1949 *Atomic Energy Levels* NBS Circular No 467, vol 1 (Washington, DC: US Govt Printing Office)

Moore D L and Norcross D W 1974 *Phys. Rev. A* **10** 1646-57

Stewart R F, Laughlin C and Victor G A 1974 *Chem. Phys. Lett.* **29** 353-8

Victor G A and Laughlin C 1972 *Chem. Phys. Lett.* **14** 74-6